The Evolution of Total Internal Reflection Raman Spectroscopy for the Chemical Characterization of Thin Films and Interfaces

Charles K. A. Nyamekye [1, 2] • Jonathan M. Bobbitt [1, 2] • Qiaochu Zhu [1] • Emily A. Smith [*, 1, 2]

[1] Department of Chemistry, Iowa State University, Ames, Iowa 50011, United States

[2] U.S. Department of Energy, The Ames Laboratory, Ames, IA, 50011, United States

[*] Corresponding author. 2415 Osborn Drive, Ames, 50011, United States

Email address: esmith1@iastate.edu (E. A. Smith)

ORCID ID

Charles K. A. Nyamekye: 0000-0002-5190-3213

Jonathan M. Bobbitt: 0000-0003-4639-1038

Qiaochu Zhu: 0000-0002-1187-1608

Emily A. Smith: 0000-0001-7438-7808

Abstract

Total internal reflection (TIR) optical spectroscopies have been widely used for decades as non-destructive and surface-sensitive measurements of thin films and interfaces. Under TIR conditions, an evanescent wave propagates into the sample layer within a region approximately 50 nm to 2 μm from the interface, which limits the spatial extent of the optical signal. The most common TIR optical spectroscopies are fluorescence (i.e., TIRF) and infrared spectroscopy (i.e., attenuated total reflection infrared). Despite the first report of TIR Raman spectroscopy appearing in 1973, this method has not received the same attention to date. While TIR Raman methods can provide chemical specific information, it has been outshined in many respects by surface-enhanced Raman spectroscopy (SERS). TIR Raman spectroscopy, however, is garnering more interest for analyzing the chemical and physical properties of thin polymer films, self-assembled monolayers (SAMs), multilayered systems, and adsorption at an interface. Herein we discuss the early experimental and computational work that laid the foundation for recent developments in the use of TIR Raman techniques. Recent applications of TIR Raman spectroscopy as well as modern TIR instruments capable of measuring monolayer-sensitive vibrational modes on smooth metallic surfaces are also discussed. The use of TIR Raman spectroscopy has been on a rise and will continue to push the limits for chemical specific interfacial and thin film measurements.

Keywords

vibrational spectroscopy, thin film characterization, polymer characterization, waveguide spectroscopy, optical spectroscopy

Abbreviations

ATR	Attenuated total reflection
PWR	Plasmon waveguide resonance
SA	Scanning angle
SERS	Surface-enhanced Raman spectroscopy
SPP	Surface plasmon polariton
SPR	Surface plasmon resonance
TIR	Total internal reflection

Introduction

The chemical characterization of surfaces and interfaces is indispensable for state-of-the-art research in separations, heterogeneous catalysis, energy harvesting and storage devices, and electrochemistry. In order to understand the properties of interfaces, many destructive and non-destructive microscopic and spectroscopic methods have been extensively deployed. Electron microscopy techniques and scanning probe microscopies (e.g., atomic force microscopy) can provide primarily structural information about an interface with atomic spatial resolution. While these techniques offer an unrivalled spatial resolution, they provide limited chemical information. They also have a limited ability to measure dynamic information and structural information below the top-most surface layer without destructive sample preparation methods.

Total internal reflection (TIR) vibrational spectroscopies (e.g., attenuated total reflection infrared spectroscopy and TIR Raman spectroscopy) can non-destructively measure chemical composition and molecular orientation at an interface with minimal sample preparation. TIR vibrational spectroscopies, like other TIR optical spectroscopies, use evanescent waves to provide interfacial selectivity and sensitivity. The fundamental principles behind TIR Raman spectroscopy have been reviewed by Bain et al. [1-3]. Briefly, the TIR phenomena occurs at an interface between two dielectric materials of differing indices of refraction: η_1 (for the total internal reflection element or prism) and η_2 (for the sample), where η_1 is greater than η_2. The incident light travels from the dielectric material with a higher refractive index to the lower refractive index material at an angle greater than or equal to the critical angle θ_c, as described by Snell's law:

$$\theta_c = sin^{-1}\left(\frac{\eta_2}{\eta_1}\right) \tag{1}$$

At the critical angle, there is no transmitted wave that propagates through the sample η_2, but there is an evanescent wave generated at both sides of the interface. The evanescent wave travels parallel to the interface and exponentially decays from the interface. The penetration depth of the evanescent wave, d_p, is where the intensity drops to a value of 1/e, and on the sample side is given by:

$$d_p = \frac{\lambda_0}{2\pi}\frac{1}{\sqrt{\eta_1^2 sin^2\theta_i - \eta_2^2}} \tag{2}$$

where λ_0 is the wavelength of light with an incident angle θ_i. The properties of the evanescent wave confine the measured vibrational signals to the interface. Comparing TIR Raman and infrared signals, in addition to different selection rules, Raman spectroscopies have the benefit of using shorter wavelengths of light. This results in a smaller penetration depth of the evanescent wave and an increased surface sensitivity. Also, the penetration depth of the evanescent wave varies across the infrared spectrum because the excitation wavelength is varied to collect the absorption spectrum. Raman scattering produces minimal spectral interference from

peaks associated with water, and maybe better suited for aqueous samples. On the other hand, IR signals generally result in better detection limits. Table 1 summarizes key similarities and differences between ATR-IR and TIR Raman spectroscopies, and serves as a guide to when either technique may be preferred.

Table 1 Selected comparisons of attenuated total reflection infrared (ATR-IR) and total internal reflection (TIR) Raman spectroscopies

ATR-IR	TIR Raman
Requires a change in the dipole moment	Requires a change in polarizability
Adsorption of IR radiation	Inelastic scattering (measures relative frequencies)
Excitation light in mid-IR region, reflective optics generally required	Range of excitation wavelengths may be used (UV, visible, or IR)
d_p varies with the excitation wavelength, which may complicate ATR-IR depth profiling measurements	A single excitation wavelength is used, which may simplify depth profiling measurements
d_p is generally greater than 1 μm	d_p is generally in the range of 100 nm to 1 μm
Water background from sample may be problematic	Fluorescence background from sample or prism may be problematic
Collected spectral range often dependent on the ATR crystal (ex: diamond 45,000-10 cm^{-1}; α-Al_2O_3 50,000-1,780 cm^{-1}; ZnSe 20,000-650 cm^{-1}; Ge 5,500-830 cm^{-1})	Possible to measure low Raman shifts with many prism types
Signal enhancement is generally not needed	Raman scattering signal may be low, signal enhancement may be required
Commercial instruments are readily available	Home-built instruments currently in use
Measurement of all types of samples including organic and inorganic solids, liquids, powders, pastes, gases, as well as biological specimens	
Self-assembled monolayer detection has been reported	
Real-time adsorption measurements can be performed	

Even though the first reports of TIR Raman spectroscopy occurred approximately a half century ago, relatively few papers have been published covering TIR Raman spectroscopy compared to other TIR optical spectroscopies. This is partly due to the discovery and subsequent focus on surface-enhanced Raman spectroscopy (SERS) [4-8]. While SERS measured at a roughened noble metal surface provides large signal enhancements, it has drawbacks for some applications. These include: a signal enhancement that can only be achieved at a couple of nanometers distance away from the plasmon-supporting surface, thus limiting the distance over which the signal can be achieved and the thickness of the sample that can be studied; and the need for a roughened substrate, which prohibits the study of smooth films, such as those found in many electronic devices (e.g., polymer-based organic light-emitting diodes and organic solar cells) [9,10]. (Similarly, tip-enhanced Raman spectroscopy can also be used to study interfaces, but for some applications, it has the disadvantages of SERS as well as other scanning probe microscopies).

In this review, the fundamental work that paved the way for recent advances in TIR Raman spectroscopy is briefly outlined [11-20]. In recent years, TIR Raman spectroscopy has received renewed interest due in part to improvements in Raman instrumentation that have expanded the types of samples that can be

studied [21-27]. Recent advances and applications of TIR Raman spectroscopy will also be covered including studies of thin polymer films [28-35], SAMs [2,36], phospholipid bilayers at liquid interfaces [25], and hydrogen bonding at silica/water or ice interfaces [24]. TIR Raman spectroscopies have been combined with smooth [37-43] and rough [44,45,40,46,47] noble metal substrates for signal enhancement; the latter is equivalent to SERS under TIR conditions. Only the former will be covered in detail in this review.

Modeling the TIR Raman Signal

Prior to the first experimental demonstration of TIR Raman spectroscopy, the appropriate theory for modeling the signal was reported. The reflected light from the interface can be modeled by Fresnel reflectivity coefficients, R_p and R_s, where the subscript refers to the polarization of the incident light. P-polarized light has an electric field oriented parallel to the plane of incidence and s-polarized light has an electric field perpendicular to that plane. Fig. 1a shows the Fresnel reflectivity curves as a function of the incident angle at a sapphire prism/organic layer interface. As expected, the 57.551° critical angle for this interface is marked by a sharp increase in the reflected light intensity. Hansen [14] derived the equations for the electric field intensity under conditions of TIR illumination in two-, three-, or multi-layered systems. The oscillation of the produced electric field in the x and z directions results from p-polarized incident light and the oscillations in the y plane results from s-polarized light (Fig. 1b). Thus, controlling the polarization of the light can be used to measure, for example, the orientation of molecules at an interface. The electric fields in the y and z directions are maximum at the critical angle for the sapphire prism/organic layer interface under TIR (Fig. 1b).

D'Hooge et al. [48,49] generated the theory of Raman scattering that is produced by evanescent excitation. The Raman scattering generated at the interface containing a homogenous sample is proportional to the electric field intensity within the sample and the depth over which the Raman signal is collected. At a given incident angle, the depth over which the Raman scattering is generated, D_{RS}, decreases twice as fast as the evanescent wave since the Raman scattering is proportional to the electric field intensity:

$$D_{RS} = \frac{d_p}{2} \tag{3}$$

where d_p is the penetration depth expressed in equation 2. The depth over which the Raman scattering is generated can be adjusted at different incident angles above the critical angle to perform axial depth profiling measurements (Fig. 1c). When the incident angle changes from 58° to 59°, D_{RS} changes by ~186 nm for a sapphire prism/organic layer interface. This represents an improvement compared to confocal Raman spectroscopy, which provides an axial spatial resolution of hundreds of nanometers to microns. Confocal Raman

spectroscopy is also limited in its ability to measure thin films, especially in the presence of a bulk layer that also produces a Raman signal. The axial spatial resolution at the interface can also be tuned by controlling the variables of wavelength and refractive index of the interfacial materials. Depending on these variables, the maximum D_{RS} typically ranges from tens of nanometers to a few microns.

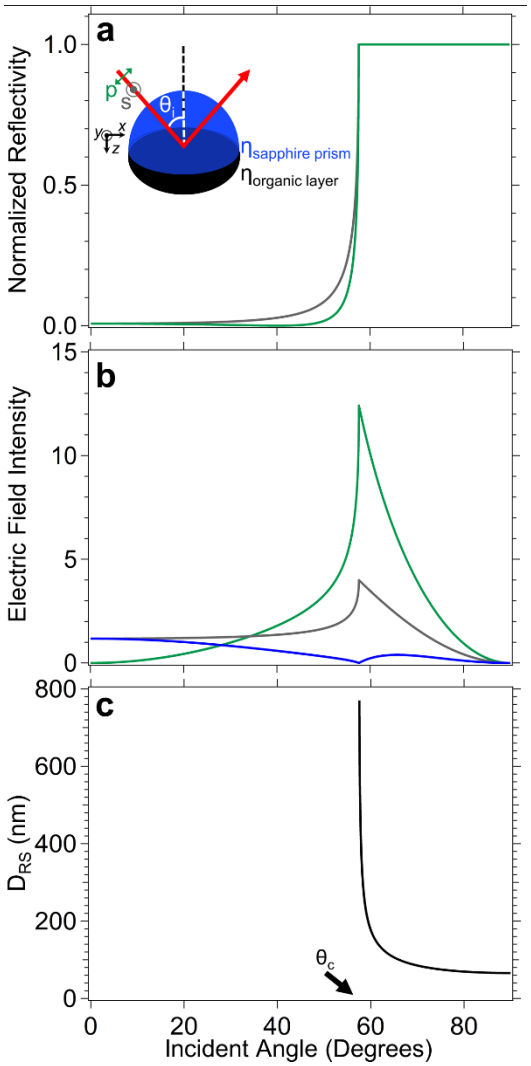

Fig. 1 Calculated **a** reflected light, **b** electric field intensity, and **c** depth over which Raman scattering is generated D_{RS} as functions of incident angle for a sapphire (η = 1.7619) / organic layer (η = 1.4868) interface at λ_0 = 785 nm. P-polarized incident light (**a**, green) produces electric fields oscillating in the x- (**b,** blue) and z-planes (**b**, green) and s-polarized incident light (**a**, gray) produces an electric field orientated in the y direction (**b**, gray). The properties of the Raman signal depend on whether it is collected on the prism side or sample side of the interface.

Experimental TIR Raman Spectroscopy

TIR Raman spectroscopy was first experimentally demonstrated by Ikeshoji et al. to analyze a liquid of carbon disulfide using a flint-glass prism [50]. Fig. 2 shows their TIR Raman spectra collected over a range of incident angles. The Raman scattering is at a maximum near the critical angle (θ_c = 70.8°) and decreases with increasing incident angle (Fig. 2a). This is due to the aforementioned decrease in the electric field intensity and D_{RS} at larger incident angles. Ikeshoji and coworkers showed that TIR Raman spectroscopy can provide an adequate signal from a solution at an interface and the ability to model the Raman scattering as the incident angle is changed.

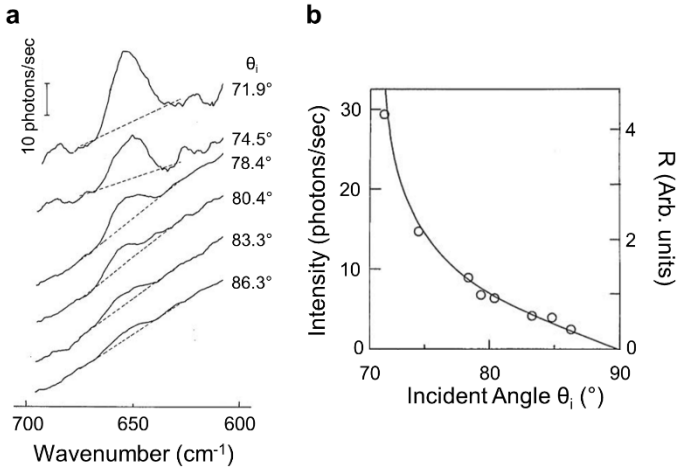

Fig. 2 a TIR Raman spectra of carbon disulfide solution (η_{sample} = 1.6180) at a hemispherical flint glass (η_{glass} = 1.7130) prism illuminated with 632.8 nm light. **b** Experimentally measured TIR Raman scattering intensities of the 654 cm^{-1} peak (symbol) and calculated fit (solid line, details of the fit can be found within the reference) as functions of incident angle. The critical angle of the hemispherical flint glass/carbon disulfide solution was 70.8°. Reprinted from [Ikeshoji T, Ono Y, Mizuno T (1973) Total Reflection Raman Spectra; Raman Scattering due to the Evanescent Wave in Total Reflection. Appl. Opt. 12 (10):2236-2237. doi:10.1364/AO.12.002236] (ref. [50]), with permission from AIP Publishing.

In 1993, Nickolov et al. used TIR Raman spectroscopy to study the O-H stretching vibrational bands of water (3200 and 3420 cm^{-1}) at two interfaces [51]. One was a hydrophobic surface composed of a 25-layer Langmuir-Blodgett film of ω-tricosenoic acid adjacent to a sapphire prism, and the second interface was a hydrophilic surface that consisted of only the sapphire prism. They concluded that the O-H Raman band changes at the hydrophobic interface compared to the hydrophilic interface due to an increase in the hydrogen bonding of water molecules at the interface with ω-tricosenoic acid.

In order to achieve high axial resolution depth profiling with TIR Raman spectroscopy, the penetration depth of the evanescent wave must be carefully controlled. This requires accurate control of the incident angle of light upon the interface. In 2010, a scanning angle (SA) Raman spectrometer with 785 nm excitation was reported for measuring interfacial phenomena with a 0.05° angle resolution using adjustable translation stages and a variable angle galvanometer mirror [52]. This angle resolution correlates to probing analytes near a planar interface with tens of nanometer spatial resolution perpendicular to the interface (i.e., axial resolution) [53-55]. As a proof of concept, this instrument was used to collect the Raman scattering from a zinc selenide prism /benzonitrile interface over a range of 35-180 nm with 1 nm axial resolution. Compared to a conventional confocal Raman microscope, the resolution of the SA Raman technique shows a 1000-fold improvement. A 532 nm SA Raman instrument was also reported (Fig. 3) that had mechanical design improvements and the benefits associated with the use of a shorter excitation wavelength (e.g., resonant enhancement, decrease in the acquisition time, and smaller D_{RS}) [56]. Resonance enhancement of the TIR Raman signal has been shown using a 532 nm laser to measure visible-light absorbing organic polymer photovoltaic films [57].

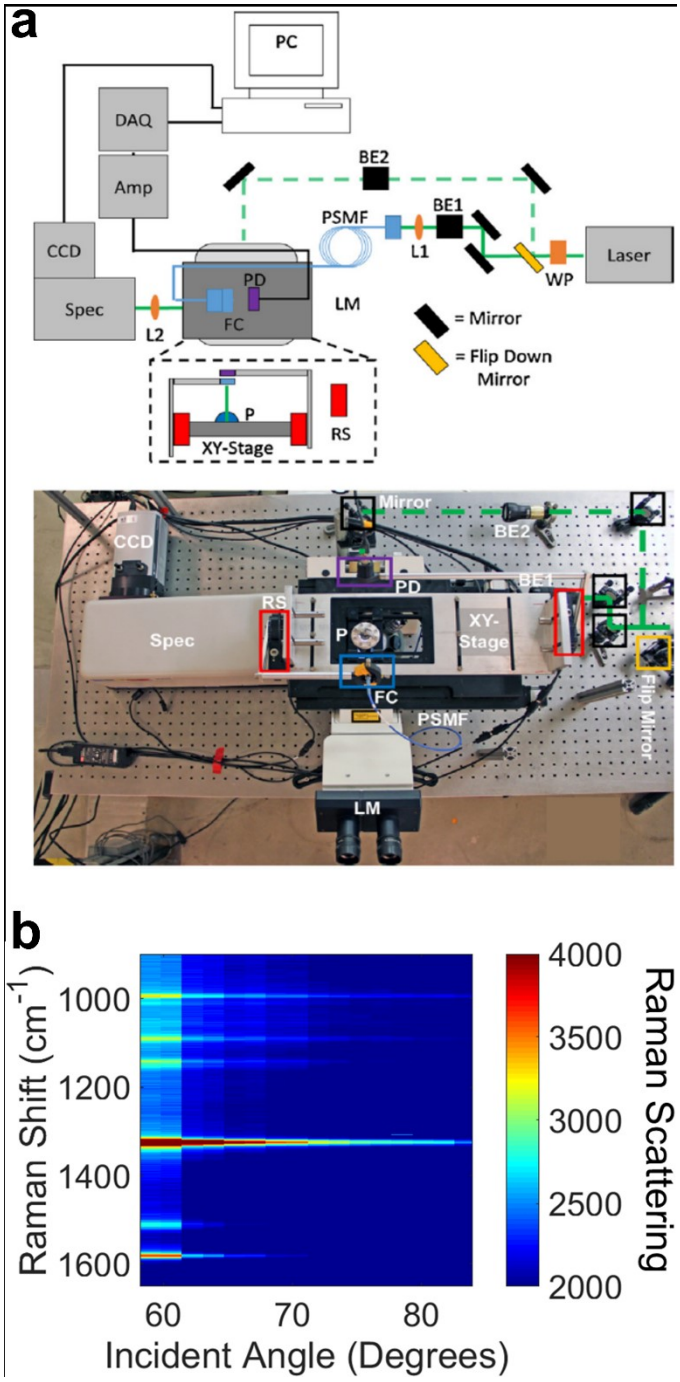

Fig. 3 a Schematic diagram and picture of a 532 nm SA Raman instrument built around an optical microscope. Amp: amplifier, BE: beam expander, CCD: charge-coupled device, DAQ: data acquisition device, FC: fiber collimator, LM: Leica microscope, L1: aspheric focusing lens, L2: collection lens, PC: computer, PSMF: polarization-maintaining single-mode fiber optic, P: prism, PD: photo-diode, RS: rotational stage, Spec: spectrometer, WP: half wave-plate. Reprinted from Anal. Chim. Acta, 848, Lesoine MD, Bobbitt JM, Zhu S, Fang N, Smith EA, High angular-resolution automated visible-wavelength scanning angle Raman microscopy, 61-66 (ref. [56]), Copyright (2014), with permission from Elsevier. **b** SA Raman spectra of nitrobenzene at a sapphire interface. The color amplitude scale represents the Raman scattering intensity. As expected, the largest

TIR Raman signal for all Raman peaks is measured near the critical angle of 61.2° and exponentially decays towards higher incident angles.

Polymer and Waveguide Samples

Polymer films are one of the most commonly studied samples using TIR Raman spectroscopy. Many of these polymer films are waveguides. A waveguide consists of a dielectric layer with a thickness greater than or equal to $\frac{\lambda_0}{2\eta_2}$, where λ_0 is the excitation wavelength and η_2 is the refractive index of the polymer. The electric field intensity calculated within a 1 μm polymer waveguide film (η_2 = 1.5099) is plotted as a function of incident angle in Fig. 4a. There is a maximum in the electric field intensity at two angles: 50° (labeled mode 1) and 57° (labeled mode 0). At both angles, the electric field intensity can be calculated as a distance across the interface (Fig. 4b, where the polymer is from 1000 to 2000 nm in this calculation). The 1 μm polymer film acts as a radiative or "leaky" waveguide, which is caused by the interference from counter propagating reflections. The number of antinodes within the waveguide layer in the electric field intensity is given by the mode integer (Fig. 4b). Since the scattering intensity is proportional to the electric field intensity, this indicates that the Raman signal is not generated uniformly throughout the waveguide. In addition, the profile of the Raman scattering generated throughout the film is different at 50° and 57°. The spatial dependence of the generated Raman signal within the waveguide film is influenced by the refractive index and thickness of the polymer as well as the excitation wavelength, incident angle, and polarization of the excitation light. Harnessing the spatial dependence of the generated Raman signal within waveguide samples as a function of incident angle, SA Raman spectroscopy can be used to determine physical properties of the waveguide such as the refractive index, thickness and composition.

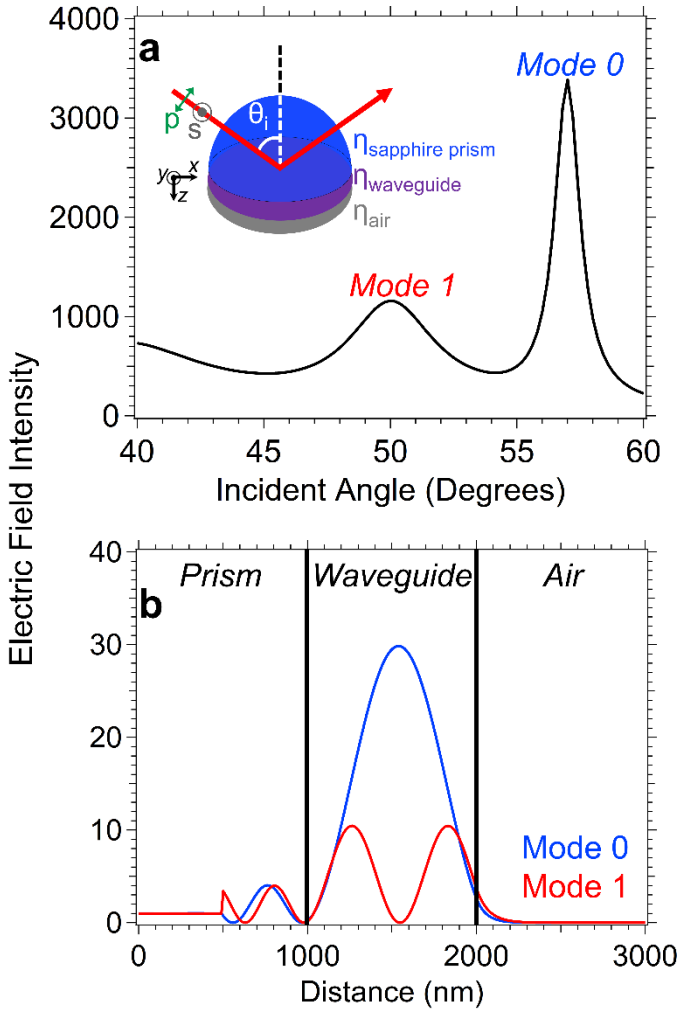

Fig. 4 Calculated electric field intensity for a 1 μm polymer waveguide film (η_2 = 1.5099) as functions of **a** the incident angle of s-polarized 785 nm light and **b** the distance from the interfacial layers. The red curve in **b** corresponds to mode one at 50° and the blue curve corresponds to mode zero at 57°. The vertical black lines represent the interface locations.

Rabolt and coworkers [58-62] studied the waveguide nature of thick polymer films and multilayered polymer films. Their initial findings showed that the excitation light can be coupled into a polymer waveguide film and produced Raman spectra with 1 to 2 orders of magnitude better signal-to-noise ratio than a bulk sample [58]. Following this study, Rabolt et al, studied bilayer films consisting of poly(methyl methacrylate) on poly(vinyl alcohol) and polystyrene on poly(vinyl alcohol) [59,63]. They calculated the electric field as a function of the distance throughout the dielectric waveguide bilayer. By controlling the incident angle of light, they excited waveguide mode 0 or 1 and collected the Raman spectra of bilayer films [59]. Subsequent work reported small molecule diffusion within the waveguide [64], and a variety of polymer types at different thicknesses and using different excitation wavelengths [60-62].

In 1980, Carius et al. applied TIR Raman spectroscopy to evaluate the degree of polymerization in a 6 μm thick polystyrene film prepared by thermal polymerization of a styrene monomer directly onto a hemispherical glass prism [65]. The TIR Raman spectra were acquired with 488 nm excitation and the incident angle was used to control the depths over which the Raman signal was collected, which was confirmed by modeling the intensities of the 3060 cm^{-1} band (CH stretch). They studied the incident angle from 67.5° to 77.5° with d_p values ranging from 125 to 400 nm. The ratios of the Raman intensities of the 1633 cm^{-1} (monomer, C=C band) and 1603 cm^{-1} (polystyrene, ring stretching mode) peaks were used to determine the ~l% monomer composition that remained after polymerization.

Also in 1980, Iwamoto et al. showed that TIR Raman spectroscopy can be used to measure a polymer bilayer film [66-68]. Fig. 5a shows the TIR Raman spectroscopy apparatus they used to collect the data for bilayer films composed of 0.05 μm polystyrene (closest to the internal reflection element) and 30 μm polyethylene (Fig. 5b). Fig. 5b reveals only peaks corresponding to polyethylene were measured when the excitation light passes straight through the sample, while the same film illuminated under TIR produced a spectrum corresponding to polystyrene. Under TIR no peaks for polyethylene were measured since its location was beyond the distance over which the Raman signal was collected [67]. Additionally, Iwamoto and coworkers [68,67] measured the Raman signal for a bilayer film as the thickness of the polymer closest to the internal reflection element increased. The TIR Raman spectra of polystyrene (closest to the internal reflection element) and polycarbonate bilayer films were collected. They showed that there is a decrease in the TIR Raman intensity ratio of the 890 cm^{-1} polycarbonate to the 1001 cm^{-1} polystyrene peaks with increasing polystyrene thickness as the polycarbonate layer moves farther away from the internal reflection element.

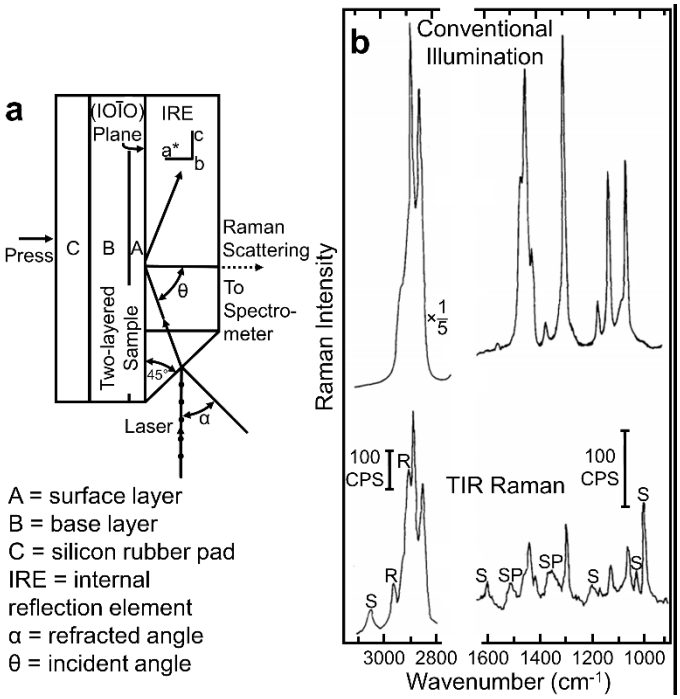

Fig. 5 a Sample configuration used to collect **b** the Raman spectra of 0.05 μm polystyrene (surface layer) coated on top of 30 μm polyethylene (base layer) film collected using (top of the figure) the conventional illumination through the sample and (bottom of the figure) the TIR illumination. The polystyrene, sapphire, and silicon rubber peaks (sample holder) are denoted with a S, SP, and R, respectively. The TIR Raman spectrum is collected at the incident angle of 64.8°. Reprinted from [Iwamoto R, Miya M, Ohta K, Mima S (1981) Total internal reflection Raman spectroscopy. J. Chem. Phys. 74 (9):4780-4790. doi:10.1063/1.441757] (ref. [67]), with the permission of AIP Publishing.

More recently, SA Raman spectroscopy with a high incident angle resolution was used to analyze solid-solid interfaces composed of blended and conjugated polymer films in organic photovoltaic devices. Meyer et al. used the SA Raman technique to measure poly(3-hexylthiophene):phenyl−C61−butyricacid methyl ester blend morphology on varying photovoltaic device substrates, such as sapphire, Au, and indium tin oxide (ITO) [69]. Compared to conventional Raman spectroscopy, the TIR Raman signals were 4× larger and enhanced at the incident angle of 35.00°. This incident angle is close to the critical angle of 34.581° for a sapphire/air interface. The authors concluded that the molecular order of poly(3-hexylthiophene) depended on the underlying substrate based on the peak width of the 1447 cm^{-1} thiophene C=C stretch, which was different for the three substrates that were studied.

Bobbitt et al. measured the chemical content and the location of buried interfaces of polymer bilayer and trilayer waveguides composed of poly(methyl methacrylate)/polystyrene and poly(methyl methacrylate)/polystyrene/poly(methyl methacrylate), respectively (Fig. 6) [70]. The thicknesses of the

poly(methyl methacrylate) layer closest to the prism and the poly(methyl methacrylate) layer farthest from the prism were varied between 160 to 420 nm in the trilayer system while the polystyrene layer was kept at a constant thickness of 180 nm. Fig. 6a-f shows the SA Raman data for trilayer films and the fit of the SA Raman signal to the electric field calculated using three-dimensional finite-difference time-domain methods. A recursive algorithm for calculating the electric field within each individual component in the multilayered film (with a 10 nm step size) was developed and used to model the SA Raman data for the bilayer and trilayer polymer films. The authors found that the SA method provided a 7 to 80 nm axial spatial resolution for probing the buried interfaces between the polymer layers in the trilayer system [70]. Furthermore, Bobbitt and coworkers simultaneously determined the refractive indices, thicknesses, and the chemical compositions of mixed polymer films consisting of polystyrene-block-poly(methyl methacrylate):poly(methyl methacrylate) at several volume ratios [71].

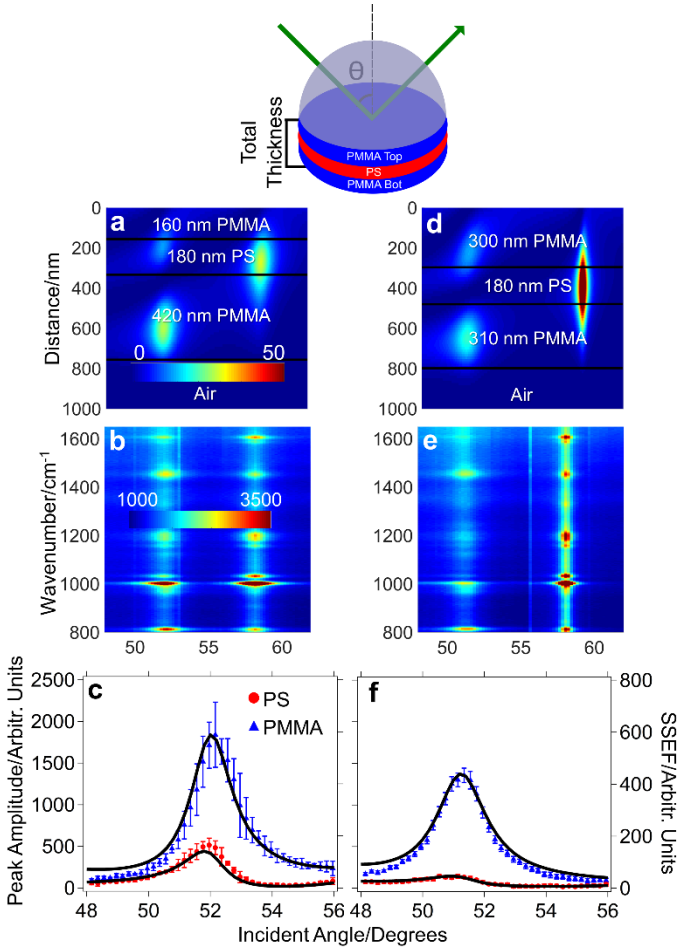

Fig. 6 Trilayer films are composed of **a-c** 160 nm poly(methyl methacrylate)/180 nm polystyrene/420 nm poly(methyl methacrylate) and **d-f** 300 nm poly(methyl methacrylate)/180 nm polystyrene/310 nm poly(methyl methacrylate). **a,d** Calculated electric field intensity plots as functions of incident angle and distance from the prism interface for the trilayer films. The color scale represents the electric field intensity. **b,e** SA Raman spectra of trilayer films with the aforementioned thicknesses plotted on a color scale representing the SA Raman scattering intensity. **c,f** Plots of the 1605 cm^{-1} polystyrene and 812 cm^{-1} poly(methyl methacrylate) peak amplitudes as a function of incident angle. The black line represents the best sum squared electric field (SSEF) fit to the experimental data. Reproduced from Bobbitt JM, Smith EA (2017) Extracting interface locations in multilayer polymer waveguide films using scanning angle Raman spectroscopy. J. Raman Spectrosc. 49 (2):262-270. doi:10.1002/jrs.5275 (ref. [70]), Copyright (2017), with permission from John Wiley and Sons.

Surface-Plasmon-Polariton-Enhanced (SPP) Raman Spectroscopy

Plasmon-supporting substrates can be incorporated into TIR Raman measurements to study phenomena occurring at the metal interface as well as to enhance the signal. Under TIR conditions, a noble metal film (e.g., Au, Ag, Pt) adjacent to a prism can support non-radiative electromagnetic surface waves (surface plasmon

polaritons, SPPs) when the electron oscillation frequency of the metal film matches the wavevector of the incident light. Only SPP Raman spectroscopies utilizing smooth planar noble metal films will be discussed herein. Burstein and collaborators in 1969 were the first to propose the use of Ag films in a TIR configuration to enhance the Raman scattering intensity of adsorbates [72]. Ushioda and collaborators used both experiment and theory to conclude that there is a significant enhancement of the Raman scattering intensity of adsorbates on a metal surface. They found a 200× increase in the Raman scattering intensity of a BK-7 prism/Ag film/pyridine sample/air interface in the Kretschmann configuration with a 514.5 nm laser beam, after finding that a 57 nm thick Ag film generated the largest electric field [73]. Furthermore, they found that the angle where propagating surface plasmons were excited in the metal film (the SPR angle) slightly differed from the angle where the highest Raman signal was generated due to the difference in the incident and scattered light energies.

Modern SPP Raman spectroscopy instruments can collect spectra as a function of incident angle with monolayer sensitivity. The SPP Raman signal of a 1.25 M pyridine solution at a Au film interface as a function of incident angle is shown in Fig. 7a [37]. The signal is well-modeled by the calculated values for the electric field and D_{RS} (Fig. 7b-d). The Raman scattering is enhanced 4-fold at the angle where SPPs are most efficiently excited in the metal film [37]. SPP Raman spectroscopy was also demonstrated by Etchegoin et al. [74] using Nile blue adsorbed on 50 nm Au and Ag films at an air interface and excited with 647 nm light. In addition, SPP Raman scattering from a smooth silver film with 532 nm excitation was used to measure a small molecule-protein interaction at the metal surface [75]. The 1631 cm^{-1} Raman band (aromatic C=C stretch) of Atto610-labeled biotin was observed upon binding to the protein avidin. Subsequently, the authors added silver colloids to generate the surface roughness required for SERS.

A limitation to measuring the Raman signal at SPP-supporting films is that only p-polarized excitation can be used to enhance the Raman signal, unless the sample is a waveguide or is adsorbed to a waveguide surface. P- and s-polarized excitation light can be used to collect Raman signals generated from waveguide modes, which can provide information about molecular orientation [76]. By scanning the incident angle of light while simultaneously collecting the Raman signal from a plasmon waveguide sample, the angle where the maximum Raman signal was generated was used to build a calibration curve for polymer thickness [77]. A follow-up of this work conducted by Bobbitt and coworkers [78], showed that a similar analysis could be performed by simultaneously scanning the incident wavelength and angle of light.

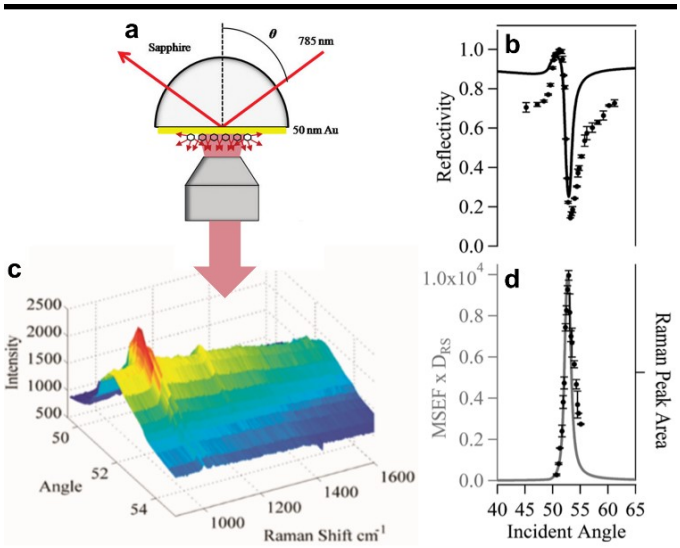

Fig. 7 a Sample geometry used to measure aqueous pyridine solution at a sapphire prism/50 nm Au/pyridine solution interface with the Raman signal collected on the sample side. **b** Experimentally measured (dotted symbol) reflected light intensity and Fresnel reflectivity calculations (solid line). **c** SPP Raman spectra of pyridine collected with 785 nm excitation. **d** Calculated mean square electric field (MSEF) × D_{RS} (gray) fit to the SPP Raman peak areas (black, symbols). Reprinted (adapted) with permission from McKee KJ, Meyer MW, Smith EA (2012) Near IR Scanning Angle Total Internal Reflection Raman Spectroscopy at Smooth Gold Films. Anal. Chem. 84 (10):4300-4306. doi:10.1021/ac203355a, (ref. [37]). Copyright (2012) American Chemical Society.

Directional Raman Scattering

Large collection efficiencies are achieved when the Raman signal is collected on the prism side of a prism/metal/sample interface under TIR conditions (Fig. 8a). This is due to the directionality of the scattered light in the form of a hollow cone, called the surface plasmon polariton (SPP) cone (Fig. 8b). Simon and Guha [79] were the first to report an experimentally measured SPP cone. They determined that the directional Raman signal collected on the prism side (Fig. 8c) was larger than the Raman signal measured on the air side. Braundmeier and Tomaschke [80] proposed two mechanisms for the generation of the SPP cone observed on a Ag film under TIR conditions: 1) momentum conserving optical coupling and 2) scattering from surface irregularities or roughness coupling [80]. The excitation of surface plasmons in the plane of the metal film (in-coupling) and the scattered light through the prism (out-coupling) results in the directional emission of the SPP cone at a sharp and defined angle. Equation 4 illustrates the incident angle θ_{inc} that results in the SPP cone, where η_1 is the refractive index of the prism and ϵ is the dielectric function of the metal film.

$$\theta_{inc} = arcsin\left[\eta_1^{-1}\left(\frac{\epsilon}{1+\epsilon}\right)^{\frac{1}{2}}\right] \quad (4)$$

Otto and coworkers experimentally demonstrated directional Raman scattering from carbon contaminates and Rhodamine 6G adsorbed on Ag films by collecting the signal from the full SPP cone radiating from a Weierstrass prism (hyperhemispherical prism) [81]. Byahut and Furtak designed an instrument to collect the directional Raman signal of *p*-nitrosodimethylaniline adsorbed on smooth and rough Ag films [82,40,83]. They showed that the highest intensity of the 1613 cm^{-1} ring stretching mode of *p*-nitrosodimethylaniline occurred at the incident angle of 44.29°, the angle where the SPP cone is generated. Futamata and coworkers [84,41,85-87] demonstrated monolayer sensitive Raman measurements of copper phthalocyanine monolayer on Au, Ag and Cu metallic substrates by means of collecting the directional Raman signal generated from the prism side of the Otto configuration (prism/air gap/metal/sample).

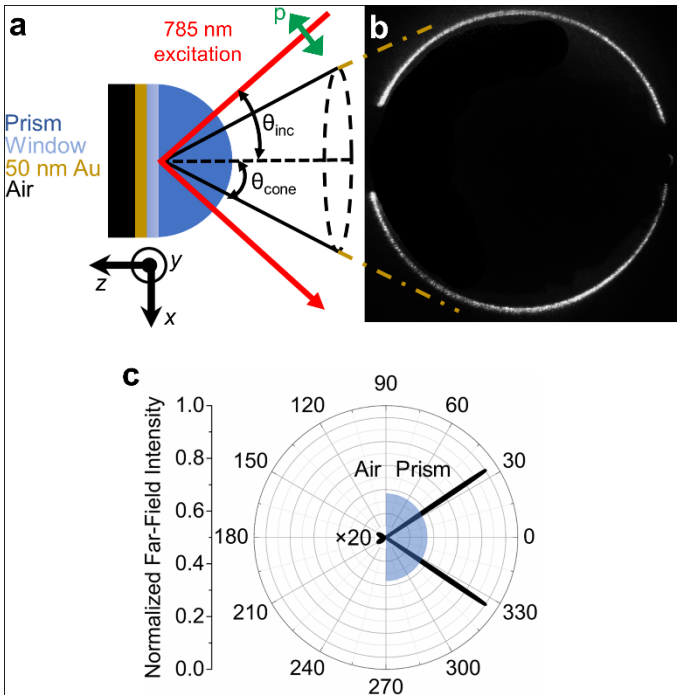

Fig. 8 a The Kretschmann configuration (hyperhemispherical prism/50 nm Au/air) used to collect **b** the surface-plasmon-polariton cone (SPP cone) acquired with a 785 nm laser at the incident angle (θ_{inc}) of 35.53°. **c** Calculated and normalized far-field angular radiation pattern depicting the directionality of the 785 nm Rayleigh scattered light through the prism. The far-field intensity on the air side was multiplied by 20.

While measurements of the SPP cone were reported by Braundmeier and Tomaschke [80] and Simon and Guha [79] in the 1970s, they did not quantify the SPP cone properties. Nyamekye and coworkers developed

a directional Raman spectroscopy instrument (Fig. 9a) capable of collecting the full Raman scattering signal generated from the SPP cone as a function of incident angle while simultaneously collecting an image of the SPP cone [38,39]. The instrument had monolayer Raman sensitivity and the SPP cone encoded the same information measured by surface plasmon resonance. Self-assembled monolayers, thin polymer films and waveguide polymer films were measured on the same instrument [38,39]. Since the instrument design utilized translational stages (as opposed to the rotational stages commonly used in SPR sensing), faster acquisition times with a 0.06° angle resolution were possible. By utilizing a smooth planar metallic film, simple and accurate models of the experimental results were possible (Fig. 9e).

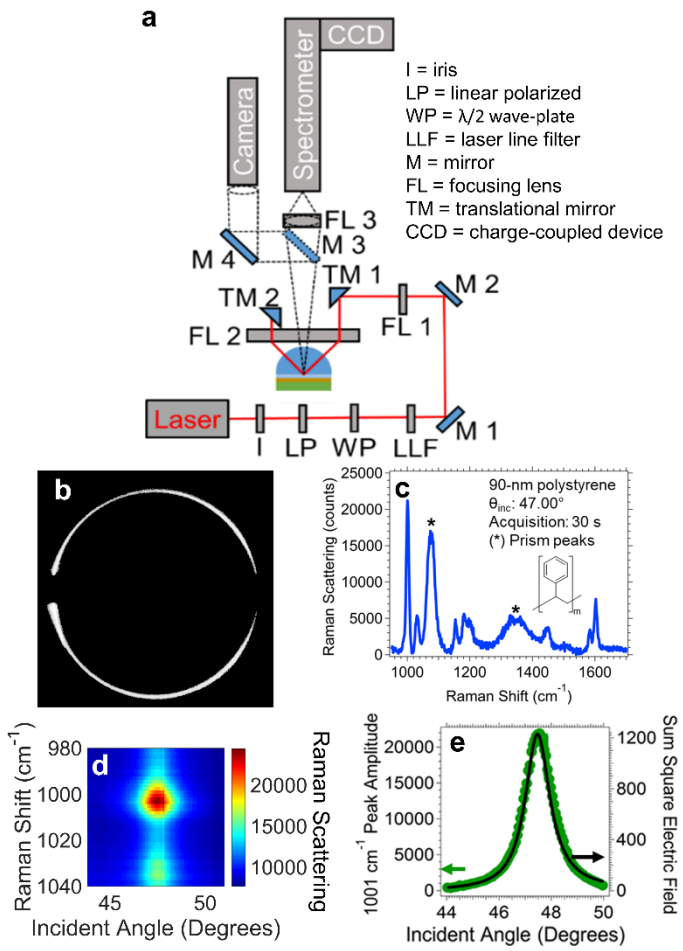

Fig. 9 a Instrument schematic of the directional Raman spectroscopy instrument. **b** An image of the SPP cone and **c** the directional Raman spectrum encoded within the cone for a 90 nm polystyrene film adsorbed on a 50 nm Au film. The SPP cone and the spectrum were acquired at the SPR angle of 47.00°. **d** Directional Raman scattering intensity as a function of Raman shift and incident angle. The color scale represents the Raman scattering intensity. **e** Peak amplitude versus incident angle of the 1001 cm^{-1} mode of polystyrene (symbol) and the calculated sum square electric field fit (solid black line) to the experimental data obtained from **d**. [Nyamekye CKA, Weibel SC, Bobbitt JM, Smith EA (2018) Combined measurement of directional Raman scattering and surface-plasmon-polariton cone from adsorbates on smooth planar gold surfaces. Analyst 143 (2):400-408. doi:10.1039/C7AN01299C] (ref. [38]) – Reproduced by permission of The Royal Society of Chemistry.

Directional Raman spectroscopy has been demonstrated by Li et al. [44] to measure a *p*-aminothiophenol monolayer adsorbed on a Ag substrate with p-polarized 532 nm excitation. They reported that the directional signal emanating through the prism at 44.5° was ~10× stronger than the Raman scattering signal on the air side. Qi and coworkers reported experimental [88,89] and calculated [90-92] directional Raman scattering from monolayers and waveguides. Neither Li nor Qi reported an experimentally measured SPP cone.

The calculations provided by Qi and coworkers, however, showed that the wavelength of the excitation source, analyte, and indices of refraction of the interfacial layers (mainly the type of metal film: Au, Ag, Pt) influenced the SPP cone properties. Most recently, Yukhymchuk and coauthors developed a directional Raman spectroscopy instrument to measure Rhodamine G6 adsorbed on Ag surfaces [93]. An elliptical mirror enabled the collection of the directional signal emanating from the full SPP cone, although the cone was not imaged. The operation of the elliptical mirror enabled a wider angular range for data collection, as opposed to using a collection lens in the instrument developed by Byahut and Furtak [40]. As with previous work, they showed the information measured is akin to that measured by surface plasmon resonance.

The directional Raman signal can also be produced by waveguide samples. Similar to the waveguide studies discussed above, the plasmon waveguide samples enable both p- and s-polarized light to generate modes in the waveguide and produce enhanced electric fields oriented in the x-, y-, and z-directions. Nyamekye et al. [39] recently reported the experimental collection and modeling of the waveguide-coupled SPP cone with reverse-Kretschmann (Fig. 10a) and Kretschmann (Fig. 10d) illumination geometries. In the reverse-Kretschmann configuration with the light illuminating the interface from the sample side and perpendicular to the interface, all the waveguide modes are excited simultaneously [91,90]. This enables the direct comparison of all the waveguide modes in a single image (Fig. 10b,c). The sensitivity (i.e., the change in the waveguide-coupled SPP cone angle per nanometer change in the polymer thickness) of all the SPP cone modes across ~400 to 700 nm polymer waveguide films is between 0.009 and 0.02° nm^{-1}. This range is similar to the plasmon waveguide resonance sensitivity value of 0.01° nm^{-1} reported by Abbas et al. [94] using an angle-scanning SPR instrument. A traditional angle scanning SPR instrument (or plasmon waveguide resonance instrument) does not provide chemical information, whereas the thickness, chemical composition, structure and orientation of thin films adsorbed onto waveguides can be obtained using the directional Raman spectroscopy instrument (Fig. 10e).

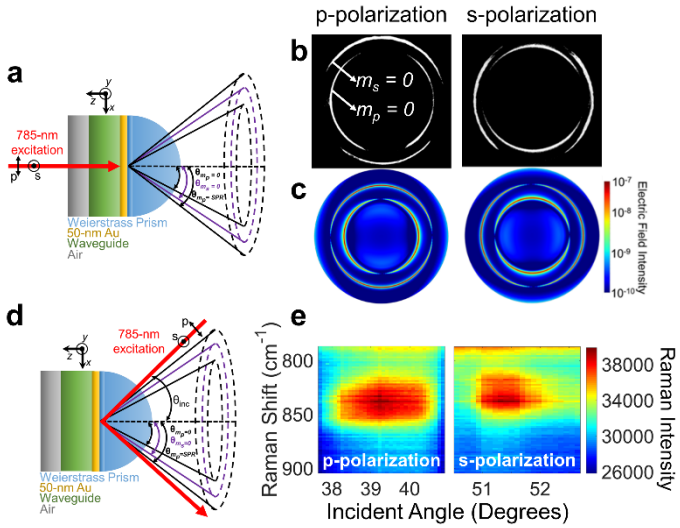

Fig. 10 a Schematic of the reverse-Kretschmann configuration used to collect **b** the experimentally measured (black/white images) and **c** calculated (color images, shown in logarithmic base 10 scale) waveguide-coupled SPP cone images of 404 nm poly(4-vinylphenol) films adsorbed onto a 50 nm Au film. The experimental [calculated] cone angles for the two waveguide modes are 35.34° [35.39°] (mode 0, p-polarization, $m_p = 0$) and 44.33° [44.30°] (mode 0, s-polarization, $m_s = 0$), respectively. **d** The Kretschmann configuration used to acquire **e** the directional Raman spectra of the 404 nm poly(4-vinylphenol) film collected as a function of the Raman shift and incident angle with p- and s-polarized 785 nm excitation. The 842 cm^{-1} Raman band is assigned to the out-of-plane CH deformation mode. Reprinted from Anal. Chim. Acta, 1048, Nyamekye CKA, Zhu Q, Mahmood R, Weibel SC, Hillier AC, Smith EA, Experimental Analysis of Waveguide-coupled Surface-plasmon-polariton Cone Properties, 123-131 (ref. [39]), Copyright (2019), with permission from Elsevier.

Concluding Remarks

From the 1970s until recently, a variety of non-destructive TIR Raman methods have been developed and improved upon for surface-sensitive measurements. TIR Raman techniques have great potential for a variety of surface and interfacial measurements, and in many cases can provide complementary information to other surface analysis techniques. The primary impediment to the adoption of the technique is the availability of commercial instruments. While most of the instruments used to collect the data discussed in this review were prism-based TIR Raman instruments, TIR Raman scattering can be excited and collected through a high numerical aperture objective lens. This is similar to most total internal reflection fluorescence (TIRF) experiments using a commercial instrument, wherein the laser is directed to the sample at an angle greater than the critical angle through the objective. Compared to using an external prism, the objective-based TIR approach generally simplifies laser alignment, and may be better suited and easily adapted to many commercial TIR

Raman instruments. The prism-based approach, on the other hand, is better suited when the index of refraction of the internal reflection element needs to be changed and to achieve a larger range of incident angles. Once the utility of the technique is accepted, more specialized commercial instrumentation may be developed.

Another area of continued research is pushing the limits of the signal to measure thinner films and lower concentrations of surface species. Of course roughened metal surfaces can be used in the TIR Raman format, and these measurements are useful in many cases, but signal enhancement strategies that maintain the smooth interface will be particularly useful. Such advancements could enable in-situ TIR Raman spectroscopy studies of, for example, photovoltaic thin films, polymer brushes, sensors, and model thin film catalysts. Furthermore, TIR Raman spectroscopy can be applicable in industrial settings, such as the automotive industry. An excellent example of this was reported by Bain and co-workers, comprising the direct TIR Raman detection of thin lubricant films in a tribological contact to evaluate shear thinning in the wear of engine components [26]. Among all previously studied samples, gas-based monitoring is the least studied with TIR Raman spectroscopy. We envision an increase in the detection of gases with TIR Raman spectroscopy, particularly with new signal enhancement strategies established. Finally, while TIR Raman spectroscopy is ideally suited for three-dimensional depth profiling and imaging at the interface, much work remains to be done to fully take advantage of its capabilities. For example, future directions may be aimed at obtaining exquisite depth profiling measurements of the Raman signal to reconstruct polymer film structures as well as imaging to obtain lateral spatial resolution. The future of TIR Raman spectroscopy will break the barriers to achieve better depth profiling resolution with fast temporal resolution to measure dynamic events as they occur at a surface.

Acknowledgements

The authors acknowledge support from the National Science Foundation under Grant Number CHE-1709099.

Disclaimer Any opinions, findings, and conclusions or recommendations expressed in this material are those of the authors and do not necessarily reflect the views of the National Science Foundation.

Compliance with ethical standards

Conflict of Interest The authors declare no competing interests.

References

1. Greene PR, Bain CD (2004) Total internal reflection Raman spectroscopy. Spectroscopy Europe 16 (4):8-15

2. Woods DA, Bain CD (2012) Total internal reflection Raman spectroscopy. Analyst 137 (1):35-48. doi:10.1039/C1AN15722A

3. Woods DA, Bain CD (2014) Total internal reflection spectroscopy for studying soft matter. Soft Matter 10 (8):1071-1096. doi:10.1039/C3SM52817K

4. Fleischmann M, Hendra PJ, McQuillan AJ (1974) Raman spectra of pyridine adsorbed at a silver electrode. Chem. Phys. Lett. 26 (2):163-166. doi:http://dx.doi.org/10.1016/0009-2614(74)85388-1

5. Allen CS, Schatz GC, Van Duyne RP (1980) Tunable laser excitation profile of surface enhanced Raman scattering from pyridine adsorbed on a copper electrode surface. Chem. Phys. Lett. 75 (2):201-205. doi:https://doi.org/10.1016/0009-2614(80)80496-9

6. Allen CS, Van Duyne RP (1981) Molecular generality of surface-enhanced Raman spectroscopy (SERS). A detailed investigation of the hexacyanoruthenate ion adsorbed on silver and copper electrodes. J. Am. Chem. Soc. 103 (25):7497-7501. doi:10.1021/ja00415a017

7. Jeanmaire DL, Van Duyne RP (1977) Surface Raman spectroelectrochemistry: Part I. Heterocyclic, aromatic, and aliphatic amines adsorbed on the anodized silver electrode. J. Electroanal. Chem. Interf. Electrochem. 84 (1):1-20. doi:https://doi.org/10.1016/S0022-0728(77)80224-6

8. Langer J, Jimenez de Aberasturi D, Aizpurua J, Alvarez-Puebla RA, Auguié B, Baumberg JJ, Bazan GC, Bell SEJ, Boisen A, Brolo AG, Choo J, Cialla-May D, Deckert V, Fabris L, Faulds K, García de Abajo FJ, Goodacre R, Graham D, Haes AJ, Haynes CL, Huck C, Itoh T, Käll M, Kneipp J, Kotov NA, Kuang H, Le Ru EC, Lee HK, Li J-F, Ling XY, Maier SA, Mayerhöfer T, Moskovits M, Murakoshi K, Nam J-M, Nie S, Ozaki Y, Pastoriza-Santos I, Perez-Juste J, Popp J, Pucci A, Reich S, Ren B, Schatz GC, Shegai T, Schlücker S, Tay L-L, Thomas KG, Tian Z-Q, Van Duyne RP, Vo-Dinh T, Wang Y, Willets KA, Xu C, Xu H, Xu Y, Yamamoto YS, Zhao B, Liz-Marzán LM (2020) Present and future of surface-enhanced Raman scattering. ACS Nano 14 (1):28-117. doi:10.1021/acsnano.9b04224

9. Fan M, Andrade GFS, Brolo AG (2011) A review on the fabrication of substrates for surface enhanced Raman spectroscopy and their applications in analytical chemistry. Anal. Chim. Acta 693 (1):7-25. doi:https://doi.org/10.1016/j.aca.2011.03.002

10. White MS, Kaltenbrunner M, Głowacki ED, Gutnichenko K, Kettlgruber G, Graz I, Aazou S, Ulbricht C, Egbe DAM, Miron MC, Major Z, Scharber MC, Sekitani T, Someya T, Bauer S, Sariciftci NS (2013) Ultrathin, highly flexible and stretchable PLEDs. Nat. Photonics 7:811. doi:10.1038/nphoton.2013.188 https://www.nature.com/articles/nphoton.2013.188#supplementary-information

11. Fahrenfort J (1961) Attenuated total reflection: A new principle for the production of useful infra-red reflection spectra of organic compounds. Spectrochim. Acta 17 (7):698-709. doi:https://doi.org/10.1016/0371-1951(61)80136-7

12. Fahrenfort (1968) Developments and applications in attenuated total reflectance. Mol. Spectrosc. Proc. Conf. 4th:111

13. Harrick NJ (1960) Surface chemistry from spectral analysis of totally internally reflected radiation*. J. Phys. Chem. 64 (9):1110-1114. doi:10.1021/j100838a005

14. Hansen WN (1968) Electric fields produced by the propagation of plane coherent electromagnetic radiation in a stratified medium. J. Opt. Soc. Am. 58 (3):380-390. doi:10.1364/JOSA.58.000380

15. Karl R (1966) Application of the attenuated total reflection (ATR) method to the infrared spectroscopic analysis of multi-layer paint films. Farbe und Lack 72 (1):13

16. Shigeyuki T (1968) Infrared analysis. Kobunshi 17 (200):1017

17. Fujiyama T, Crawford B (1968) Vibrational intensities. XXI. Some band shapes and intensities in liquid hexafluorobenzene. J. Phys. Chem. 72 (6):2174-2181. doi:10.1021/j100852a050

18. Wilks PA (1969) Internal reflectance spectroscopy II: Quantitative analysis aspects. Appl. Spectrosc. 23 (1):63-66. doi:10.1366/000370269774381201

19. Hirschfeld T (1967) Procedures for attenuated total reflection study of extremely small samples. Appl. Opt. 6 (4):715-718. doi:10.1364/AO.6.000715

20. Wilks PA, Hirschfeld T (1967) Internal reflection spectroscopy. Appl. Spectrosc. Rev. 1 (1):99-130. doi:10.1080/05704926708547582

21. Beattie DA, Larsson ML, Holmgren AR (2006) In situ total internal reflection Raman spectroscopy of surfactant adsorption at a mineral surface. Vib. Spectrosc. 41 (2):198-204. doi:http://dx.doi.org/10.1016/j.vibspec.2006.02.003

22. Woods DA, Petkov J, Bain CD (2011) Surfactant adsorption by total internal reflection Raman spectroscopy. Part III: Adsorption onto cellulose. Colloid Surf. A Physicochem. Eng. Asp. 391 (1):10-18. doi:https://doi.org/10.1016/j.colsurfa.2011.07.027

23. Grenoble Z, Baldelli S (2013) Adsorption of benzyldimethylhexadecylammonium chloride at the hydrophobic silica–water interface studied by total internal reflection Raman spectroscopy: Effects of Silica Surface Properties and Metal Salt Addition. J. Phys. Chem. B 117 (34):9882-9894. doi:10.1021/jp4015096

24. Liljeblad JFD, Furó I, Tyrode EC (2017) The premolten layer of ice next to a hydrophilic solid surface: correlating adhesion with molecular properties. Phys. Chem. Chem. Phys. 19 (1):305-317. doi:10.1039/C6CP05303C

25. Lee C, Wacklin H, Bain CD (2009) Changes in molecular composition and packing during lipid membrane reconstitution from phospholipid–surfactant micelles. Soft Matter 5 (3):568-575. doi:10.1039/B812768A

26. Praveena M, Guha K, Ravishankar A, Biswas SK, Bain CD, Jayaram V (2014) Total internal reflection Raman spectroscopy of poly(alpha-olefin) oils in a lubricated contact. RSC Adv. 4 (42):22205-22213. doi:10.1039/C4RA02261K

27. Ngo D, Baldelli S (2016) Adsorption of dimethyldodecylamine oxide and its mixtures with Triton X-100 at the hydrophilic silica/water interface studied using total internal reflection Raman spectroscopy. J. Phys. Chem. B 120 (48):12346-12357. doi:10.1021/acs.jpcb.6b08853

28. Takenaka T, Nogami K, Gotoh H, Gotoh R (1971) Studies on built-up films by means of the polarized infrared ATR spectrum I.: Built-up films of stearic acid. J. Colloid Interface Sci. 35 (3):395-402. doi:https://doi.org/10.1016/0021-9797(71)90138-X

29. Nakanaga T, Takenaka T (1977) Resonance Raman spectra of monolayers of a surface-active dye adsorbed at the oil-water interface. J. Phys. Chem. 81 (7):645-649. doi:10.1021/j100522a011

30. Takenaka T (1979) Application of Raman spectroscopy to the study of surface chemistry. Adv. Colloid Interface Sci. 11 (4):291-313. doi:https://doi.org/10.1016/0001-8686(79)80011-1

31. Giesekke EW (1983) A review of spectroscopic techniques applied to the study of interactions between minerals and reagents in flotation systems. Int. J. Miner. Process. 11 (1):19-56. doi:https://doi.org/10.1016/0301-7516(83)90043-1

32. Hölzer W, Schröter O, Richter A (1990) Raman study on surface layers and thin films by using total reflection experiments. J. Mol. Struct. 217:253-264. doi:https://doi.org/10.1016/0022-2860(90)80366-R

33. Yoshikawa M, Gotoh T, Mori Y, Iwamoto M, Ishida H (1994) Determination of anisotropic refractive indices of a single-crystal organic thin film by attenuated total reflection Raman spectroscopy. Appl. Phys. Lett. 64 (16):2096-2098. doi:10.1063/1.111694

34. Fontaine NH, Furtak TE (1997) Precise control of evanescent fields from a Gaussian beam for depth-resolved spectroscopy. J. Opt. Soc. Am. B 14 (12):3342-3348. doi:10.1364/JOSAB.14.003342

35. Fontaine NH, Furtak TE (1998) Variable-angle internal-reflection Raman spectroscopy for depth-resolved vibrational characterization of polymer thin films. Phys. Rev. B 57 (7):3807-3810. doi:10.1103/PhysRevB.57.3807

36. Ota C (2015) Investigation of the structure of water at hydrophobic and hydrophilic interfaces by angle-resolved TIR Raman spectroscopy. Phys. Chem. Chem. Phys. 17 (39):26435-26442. doi:10.1039/C5CP03581C

37. McKee KJ, Meyer MW, Smith EA (2012) Near IR scanning angle total internal reflection Raman spectroscopy at smooth gold films. Anal. Chem. 84 (10):4300-4306. doi:10.1021/ac203355a

38. Nyamekye CKA, Weibel SC, Bobbitt JM, Smith EA (2018) Combined measurement of directional Raman scattering and surface-plasmon-polariton cone from adsorbates on smooth planar gold surfaces. Analyst 143 (2):400-408. doi:10.1039/C7AN01299C

39. Nyamekye CKA, Zhu Q, Mahmood R, Weibel SC, Hillier AC, Smith EA (2019) Experimental analysis of waveguide-coupled surface-plasmon-polariton cone properties. Anal. Chim. Acta 1048:123-131. doi:https://doi.org/10.1016/j.aca.2018.09.057

40. Byahut SP, Furtak TE (1991) Surface plasmon assisted Raman scattering from electrochemically controlled adsorbates on flat, single crystal silver. Electrochim. Acta 36 (11):1879-1882. doi:https://doi.org/10.1016/0013-4686(91)85061-B

41. Futamata M (1995) Surface plasmon polariton enhanced Raman scattering from adsorbates on a "smooth" metal surface: The effect of thickness and dielectric properties of constituents. Langmuir 11 (10):3894-3901. doi:10.1021/la00010a046

42. Meyer SA, Auguié B, Le Ru EC, Etchegoin PG (2012) Combined SPR and SERS microscopy in the Kretschmann configuration. J. Phys. Chem. A 116 (3):1000-1007. doi:10.1021/jp2107507

43. Jiang S-l, Chen L, Yu X-x, Zheng H-j, Lin K, Zhang Q, Wang X-p, Luo Y (2017) Surface plasmon assisted directional Rayleigh scattering. Chin. J. Chem. Phys. 30 (2):135-138. doi:10.1063/1674-0068/30/cjcp1611204

44. Li H, Xu S, Liu Y, Gu Y, Xu W (2012) Directional emission of surface-enhanced Raman scattering based on a planar-film plasmonic antenna. Thin Solid Films 520 (18):6001-6006. doi:http://dx.doi.org/10.1016/j.tsf.2012.04.084

45. Pettinger B, Tadjeddine A, Kolb DM (1979) Enhancement in Raman intensity by use of surface plasmons. Chem. Phys. Lett. 66 (3):544-548. doi:https://doi.org/10.1016/0009-2614(79)80335-8

46. Wang H, Li H, Xu S, Zhao B, Xu W (2017) Integrated plasmon-enhanced Raman scattering (iPERS) spectroscopy. Sci. Rep. 7 (1):14630. doi:10.1038/s41598-017-15111-3

47. Huo S-X, Liu Q, Cao S-H, Cai W-P, Meng L-Y, Xie K-X, Zhai Y-Y, Zong C, Yang Z-L, Ren B, Li Y-Q (2015) Surface plasmon-coupled directional enhanced Raman scattering by means of the reverse Kretschmann configuration. J. Phys. Chem. Lett. 6 (11):2015-2019. doi:10.1021/acs.jpclett.5b00666

48. D'Hooge L, Vigoureux JM, Menu C (1981) General theory of the Raman scattering close to a plane surface. Evanescent Raman spectra. J. Chem. Phys. 74 (7):3639-3659. doi:10.1063/1.441591

49. D'Hooge L, Vigoureux JM (1979) Evanescent field excitation of homogeneous raman scattering close to a dielectric. Chem. Phys. Lett. 65 (3):500-506. doi:https://doi.org/10.1016/0009-2614(79)80280-8

50. Ikeshoji T, Ono Y, Mizuno T (1973) Total reflection Raman spectra; Raman scattering due to the evanescent wave in total reflection. Appl. Opt. 12 (10):2236-2237. doi:10.1364/AO.12.002236

51. Nickolov ZS, Earnshaw JC, McGarvey JJ (1993) Water structure at interfaces studied by total internal reflection Raman spectroscopy. Colloid Surf. A Physicochem. Eng. Asp. 76:41-49. doi:https://doi.org/10.1016/0927-7757(93)80059-N

52. McKee KJ, Smith EA (2010) Development of a scanning angle total internal reflection Raman spectrometer. Rev. Sci. Instrum. 81 (4):043106. doi:10.1063/1.3378682

53. Fujiwara K, Watarai H (2003) Total internal reflection resonance Raman microspectroscopy for the liquid/liquid interface. Ion-association adsorption of cationic Mn(III) porphine. Langmuir 19 (7):2658-2664. doi:10.1021/la026119y

54. Jubb AM, Verreault D, Posner R, Criscenti LJ, Katz LE, Allen HC (2013) Sulfate adsorption at the buried hematite/solution interface investigated using total internal reflection (TIR)-Raman spectroscopy. J. Colloid Interface Sci. 400:140-146. doi:10.1016/j.jcis.2013.02.031

55. Damin CA, Nguyen VHT, Niyibizi AS, Smith EA (2015) Application of scanning angle Raman spectroscopy for determining the location of buried polymer interfaces with tens of nanometer precision. Analyst 140 (6):1955-1964. doi:10.1039/C4AN02240H

56. Lesoine MD, Bobbitt JM, Zhu S, Fang N, Smith EA (2014) High angular-resolution automated visible-wavelength scanning angle Raman microscopy. Anal. Chim. Acta 848:61-66. doi:http://dx.doi.org/10.1016/j.aca.2014.07.040

57. Lesoine MD, Bobbitt JM, Carr JA, Elshobaki M, Chaudhary S, Smith EA (2014) Quantitative comparison of organic photovoltaic bulk heterojunction photostability under laser illumination. J. Phys. Chem. C 118 (51):30229-30237. doi:10.1021/jp509589g

58. Rabolt JF, Santo R, Swalen JD (1979) Raman spectroscopy of thin polymer films using integrated optical techniques. Appl. Spectrosc. 33 (6):549-551. doi:10.1366/0003702794925101

59. Rabolt JF, Schlotter NE, Swalen JD (1981) Spectroscopic studies of thin film polymer laminates using Raman spectroscopy and integrated optics. J. Phys. Chem. 85 (26):4141-4144. doi:10.1021/j150626a038

60. Schlotter NE, Rabolt JF (1984) Raman spectroscopy in polymeric thin film optical waveguides. 1. Polarized measurements and orientational effects in two-dimensional films. J. Phys. Chem. 88 (10):2062-2067. doi:10.1021/j150654a025

61. Zimba CG, Rabolt JF (1991) Parametric optimization of waveguide Raman spectroscopy in the near-IR. Thin Solid Films 206 (1):388-393. doi:https://doi.org/10.1016/0040-6090(91)90456-8

62. Zimba CG, Turrell S, Swalen JD, Hallmark VM, Rabolt JF (1990) Applications of Fourier transform Raman spectroscopy to studies of thin polymer films. J. Phys. Chem. 94 (2):939-943. doi:10.1021/j100365a080

63. Swalen JD, Schlotter NE, Santo R, Rabolt JF (1981) Raman spectroscopy of laminated polymer films by integrated optical techniques. J. Adhes. 13 (2):189-194. doi:10.1080/00218468108073185

64. Schlotter NE (1990) Diffusion of small molecules in glassy polymer thin films studied by waveguide Raman techniques. J. Phys. Chem. 94 (4):1692-1699. doi:10.1021/j100367a086

65. Carius W, Schröter O (1980) Total reflection Raman spectroscopy (TRRS) of polystyrene. Phys. Status Solidi A 59 (1):K115-K118. doi:10.1002/pssa.2210590178

66. Iwamoto R, Miya M, Ohta K, Mima S (1980) Total internal reflection Raman spectroscopy as a new tool for surface analysis. J. Am. Chem. Soc. 102 (3):1212-1213. doi:10.1021/ja00523a074

67. Iwamoto R, Miya M, Ohta K, Mima S (1981) Total internal reflection Raman spectroscopy. J. Chem. Phys. 74 (9):4780-4790. doi:10.1063/1.441757

68. Iwamoto R, Ohta K, Miya M, Mima S (1981) Total internal reflection Raman spectroscopy at the critical angle for Raman measurements of thin films. Appl. Spectrosc. 35 (6):584-587

69. Meyer MW, Larson KL, Mahadevapuram RC, Lesoine MD, Carr JA, Chaudhary S, Smith EA (2013) Scanning angle Raman spectroscopy of poly(3-hexylthiophene)-based films on indium tin oxide, gold, and sapphire surfaces. ACS Appl. Mater. Interfaces 5 (17):8686-8693. doi:10.1021/am4023225

70. Bobbitt JM, Smith EA (2018) Extracting interface locations in multilayer polymer waveguide films using scanning angle Raman spectroscopy. J. Raman Spectrosc. 49 (2):262-270. doi:10.1002/jrs.5275

71. Bobbitt JM, Mendivelso-Pérez D, Smith EA (2016) Scanning angle Raman spectroscopy: A nondestructive method for simultaneously determining mixed polymer fractional composition and film thickness. Polymer 107:82-88. doi:http://dx.doi.org/10.1016/j.polymer.2016.10.063

72. Chen YJ, Chen WP, Burstein E (1976) Surface-electromagnetic-wave-enhanced Raman scattering by overlayers on metals. Phys. Rev. Lett. 36 (20):1207-1210

73. Giergiel J, Reed CE, Hemminger JC, Ushioda S (1988) Surface plasmon polariton enhancement of Raman scattering in a Kretschmann geometry. J. Phys. Chem. 92 (19):5357-5365. doi:10.1021/j100330a009

74. Meyer SA, Le Ru EC, Etchegoin PG (2011) Combining surface plasmon resonance (SPR) spectroscopy with surface-enhanced Raman scattering (SERS). Anal. Chem. 83 (6):2337-2344. doi:10.1021/ac103273r

75. Fu C, Hu C, Liu Y, Xu S, Xu W (2012) Bioidentification of biotin/avidin using surface plasmon resonance and surface-enhanced Raman scattering (SPR-SERS) spectroscopy. Anal. Methods 4 (10):3107-3110. doi:10.1039/C2AY25697E

76. McKee KJ, Meyer MW, Smith EA (2012) Plasmon waveguide resonance Raman spectroscopy. Anal. Chem. 84 (21):9049-9055. doi:10.1021/ac3013972

77. Meyer MW, McKee KJ, Nguyen VHT, Smith EA (2012) Scanning angle plasmon waveguide resonance Raman spectroscopy for the analysis of thin polystyrene films. J. Phys. Chem. C 116 (47):24987-24992. doi:10.1021/jp308882w

78. Bobbitt JM, Weibel SC, Elshobaki M, Chaudhary S, Smith EA (2014) Fourier transform-plasmon waveguide spectroscopy: A nondestructive multifrequency method for simultaneously determining polymer thickness and apparent index of refraction. Anal. Chem. 86 (24):11957-11961. doi:10.1021/ac504103g

79. Simon HJ, Guha JK (1976) Directional surface plasmon scattering from silver films. Opt. Commun. 18 (3):391-394. doi:http://dx.doi.org/10.1016/0030-4018(76)90158-9

80. Braundmeier AJ, Tomaschke HE (1975) Observation of the simultaneous emission of roughness-coupled and optical-coupled surface plasmon radiation from silver. Opt. Commun. 14 (1):99-103. doi:http://dx.doi.org/10.1016/0030-4018(75)90067-X

81. Wittke W, Hatta A, Otto A (1989) Efficient use of the surface plasmon polariton resonance in light scattering from adsorbates. Appl. Phys. A 48 (3):289-294. doi:10.1007/bf00619400

82. Byahut S, Furtak TE (1990) A device for performing surface-plasmon-polariton-assisted Raman scattering from adsorbates on single-crystal silver surfaces. Rev. Sci. Instrum. 61 (1):27-32. doi:10.1063/1.1141321

83. Byahut S, Furtak TE (1991) Direct comparison of the chemical properties of single crystal Ag(111) and electrochemically roughened Ag as substrates for surface Raman scattering. Langmuir 7 (3):508-513. doi:10.1021/la00051a016

84. Futamata M (1995) Surface-plasmon-polariton-enhanced Raman scattering from self-assembled monolayers of p-nitrothiophenol and p-aminothiophenol on silver. J. Phys. Chem. 99 (31):11901-11908. doi:10.1021/j100031a018

85. Futamata M (1997) Application of attenuated total reflection surface-plasmon-polariton Raman spectroscopy to gold and copper. Appl. Opt. 36 (1):364-375. doi:10.1364/AO.36.000364

86. Futamata M, Borthen P, Thomassen J, Schumacher D, Otto A (1994) Application of an ATR method in Raman spectroscopy. Appl. Spectrosc. 48 (2):252-260

87. Futamata M, Keim E, Bruckbauer A, Schumacher D, Otto A (1996) Enhanced Raman scattering from copper phthalocyanine on Pt by use of a Weierstrass prism. Appl. Surf. Sci. 100:60-63. doi:http://dx.doi.org/10.1016/0169-4332(96)00257-7

88. Wan X-m, Chen C, Fan Z-b, Lu D-f, Qi Z-m (2016) Raman spectroscopy based on plasmon waveguide prepared with mesoporous TiO_2 thin film. Acta Phys. Sin. 65:137801. doi:10.7498/aps.65.137801

89. Wan X-m, Gao R, Lu D-f, Qi Z-m (2018) Self-referenced directional enhanced Raman scattering using plasmon waveguide resonance for surface and bulk sensing. Appl. Phys. Lett. 112 (4):041906. doi:10.1063/1.5009491

90. Chen C, Lu D-f, Gao R, Qi Z-m (2016) Analysis of waveguide-coupled directional emission for efficient collection of fluorescence/Raman light from surface. Opt. Commun. 367:86-94. doi:http://dx.doi.org/10.1016/j.optcom.2016.01.001

91. Chen C, Li J-Y, Wang L, Lu D-f, Qi Z-m (2015) Waveguide-coupled directional Raman radiation for surface analysis. Phys. Chem. Chem. Phys. 17 (33):21278-21287. doi:10.1039/C4CP05092D

92. Chen C, Lu D-f, Ran G, Jin C, Qi Z-m (2016) Surface Raman spectroscopy with and without reverse Kretschmann configuration: Effect of evanescent-wave-coupled emission. Appl. Phys. Express 9 (6):062001

93. Beketov GV, Shynkarenko OV, Yukhymchuk VO (2019) Optical arrangement for surface plasmon-assisted directional enhanced Raman scattering spectroscopy. Spectrochim. Acta Part A: Molecular and Biomolecular Spectroscopy 219:488-495. doi:https://doi.org/10.1016/j.saa.2019.04.039

94. Abbas A, Linman MJ, Cheng Q (2011) Sensitivity comparison of surface plasmon resonance and plasmon-waveguide resonance biosensors. Sens. Actuators, B 156 (1):169-175. doi:https://doi.org/10.1016/j.snb.2011.04.008

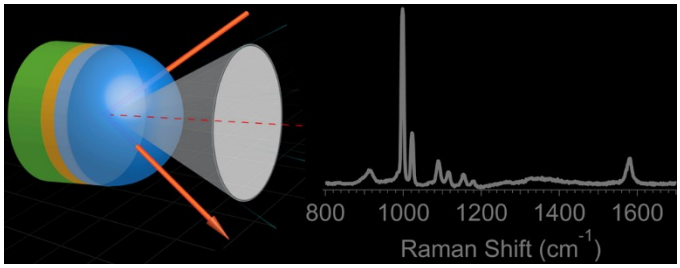

Total internal reflection (TIR) Raman spectroscopy can extract the chemical and physical information from thin films and adsorbates.